Progress In Electromagnetics Research C, Vol. 172, 231–241, 2026

PIER C

(Received 17 June 2026, Accepted 15 July 2026, Scheduled 10 August 2026)

A Quad-Notch Ultra-Wideband Filter Based on a Bowtie T-Shaped Resonator

Mingming Gao[1,2], Ke Li[2,*], and Maoyuan Wei[2]

[1]*Ordos Research Institute, Liaoning University of Technology, Ordos 017000, Inner Mongolia, China*
[2]*School of Electronic and Information Engineering, Liaoning University of Technology, Huludao 125105, China*

ABSTRACT: To suppress multiple narrowband interferences in ultra-wideband (UWB) communication systems while maintaining a compact size and wide passband response, a quad-notch UWB filter based on a bowtie T-shaped resonator is proposed and investigated. The proposed filter employs an improved stepped-impedance resonator (SIR) with multi-branch loading and an annular defected ground structure (DGS) to enhance bandwidth extension, passband flatness, and frequency selectivity. A novel quasi-closed-loop C-shaped resonator with an additional coupling path is introduced to generate an extra controllable resonant mode, providing enhanced flexibility for independent notch-band tuning. Combined with an asymmetric open-circuited branch, four independently adjustable notch bands are achieved within the UWB passband. Resonance characteristics of the proposed multimode structure are analyzed using even-odd mode theory, providing an effective approach for mode-frequency control. Experimental results demonstrate that the fabricated filter achieves a wide passband from 2.71 to 11.5 GHz with a fractional bandwidth of 124%, along with four sharp rejection bands centered at 5.91, 6.75, 7.29, and 8.08 GHz. The maximum attenuation reaches 34.55 dB, while the filter maintains a compact size of 23 mm $\times$ 29.74 mm with excellent passband flatness and out-of-band suppression. The proposed quad-notch UWB filter provides an effective solution for interference-resistant wireless communication systems.

1. INTRODUCTION

Presently, multimode resonators are extensively employed in broadband and ultra-wideband (UWB) filters. The inherent independence of the multiple resonance modes within a single multimode resonator facilitates substantial reduction in the required number of resonant elements. Consequently, this characteristic minimizes both the circuit footprint and overall physical dimensions, establishing the multimode approach as a pivotal technology for the miniaturization of UWB filters [1]. To generate multiple discrete passbands or resonances, traditional approaches often rely on coupled, cascaded, or periodic cavity arrangements; however, these configurations typically occupy substantial physical space and suffer from significant transmission throughput degradation due to compounding cascading losses. To overcome these spatial limitations, contemporary designs leverage advanced single-cavity geometries to exploit a rich mode spectrum via extended optical paths and spatial mode folding within an ultra-compact footprint. Crucially, such architectures naturally separate spectral and spatial degrees of freedom, allowing for independent, mode-selective spectral tunability via structural parameters and successfully overcoming uniform scaling constraints inherent to conventional ring, disk, or stub resonators.

In ultra-wideband (UWB) systems, filters are conventionally situated at the front end to handle signal processing [2]. Such components necessitate compact form factors and cost efficiency, coupled with exceptionally broad bandwidth, minimal insertion loss, and superior frequency skirt selectivity. Consequently, the concurrent realization of high performance and miniaturization constitutes a paramount research focus in this domain. To optimize front-end architectures and reduce overall system size, modern methodologies place heavy emphasis on structural miniaturization and functional integration, such as co-designing filtering and radiation features to avoid separate components and eliminate additional unwanted interferences. Beyond these prerequisites, interference rejection has emerged as a critical performance metric for UWB systems. The rapid proliferation of wireless communication technologies has introduced substantial fixed-band interference, notably from WiMAX and WLAN signals, into the UWB spectrum [3]. Consequently, incorporating multi-notch characteristics into UWB filters constitutes an effective strategy for mitigating these in-band interferences. Although dual- and triple-notch configurations are prevalent in the literature, quad-notch UWB filters with highly independent mode optimization remain comparatively scarce in both theoretical simulation and experimental validation.

This paper proposes a quad-notch UWB filter based on a bowtie T-shaped resonator. Initially, the structure's resonant characteristics are analyzed to develop a foundational UWB filter with enhanced band selectivity and an expanded passband. Building upon this baseline design, four in-band notches are introduced by integrating supplementary branches and dedicated notch resonators, which generate one and three notches, respectively. The geometric parameters of these resonating elements are systematically optimized to ensure independent operation

* Corresponding author: Ke Li (chmeu1211@163.com).

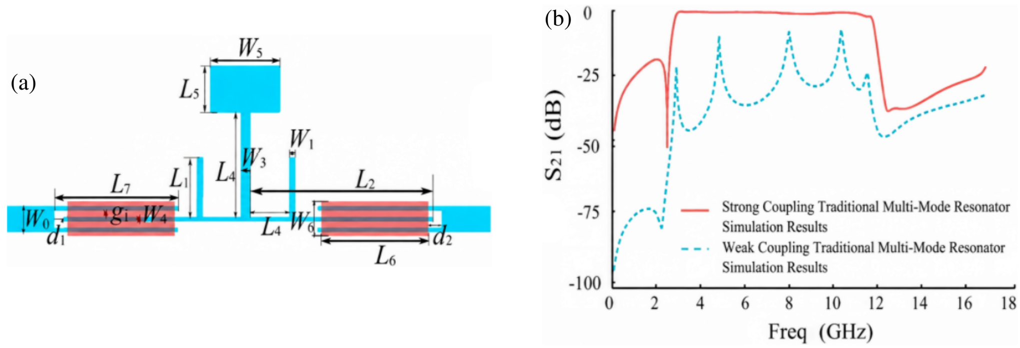

FIGURE 1. Schematic diagram of a traditional multimode resonator and its simulation results. (a) Schematic diagram and (b) simulation results.

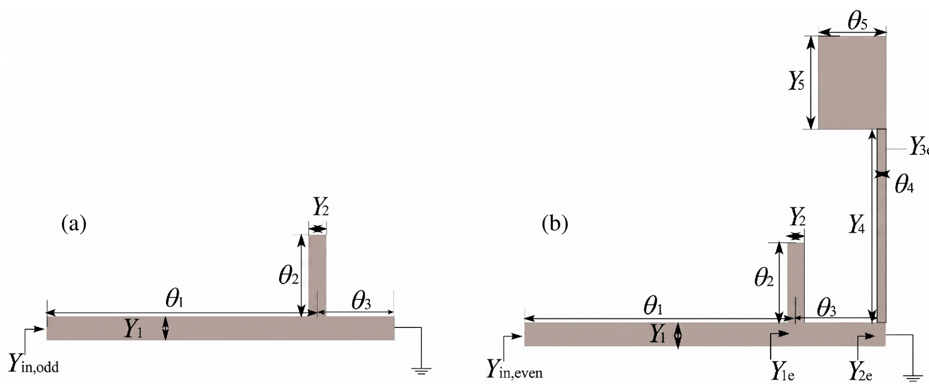

FIGURE 2. Equivalent circuit of the SIR parity mode with a single branch loaded. (a) Odd-mode equivalent and (b) even-mode equivalent.

without mutual interference. Finally, a physical prototype was fabricated and experimentally characterized. The measured results exhibit strong agreement with the simulations, thereby validating the feasibility of the proposed approach.

2. ULTRA-WIDEBAND FILTER BASED ON A BOWTIE-TYPE MULTIMODE RESONATOR DESIGN

Existing literature [4] presents an ultra-wideband (UWB) bandpass filter based on a five-mode resonator, designated as a conventional multimode resonator. The optimized physical layout and corresponding simulation results of this filter are depicted in Fig. 1(a). Structurally, the conventional multimode resonator employs a single-branch-loaded stepped-impedance resonator (SIR) configuration. Specifically, it comprises a centrally positioned SIR (L_2, L_3, W_2, W_3) that is symmetrically loaded with a single branch (L_1, W_1) on each side. Additionally, the microstrip feeding network uses an interdigital coupling structure. To enhance the coupling performance of the microstrip line, a defected ground structure (DGS) was integrated beneath it [5]. In contrast to configurations previously reported in the literature, the optimized design utilizes a Rogers 5880 substrate characterized by a relative permittivity of 2.2, a thickness of 0.787 mm, and a copper cladding thickness of 35 µm. Following iterative electromagnetic simulation and optimization via High Frequency Structure Simulator (HFSS) 15.0, the final physical dimensions were established as follows (in mm): $L_1 = 3.6$, $L_2 = 3.68$, $L_3 = 9.1$, $L_4 = 7.81$, $L_5 = 11.1$, $W_0 = 2.6$, $W_1 = 0.5$, $W_2 = 4.4$, $W_4 = 0.4$, $g_1 = 0.12$, $d_1 = 0.21$, $L_6 = 6.4$, $W_6 = 2.4$, and $d_2 = 0.72$.

As depicted in Fig. 1(b), the filter exhibits a 3-dB passband ranging from 2.89 to 11.93 GHz, corresponding to a fractional bandwidth of 122%. Additionally, two transmission zeros are successfully introduced at 2.58 GHz and 12.38 GHz, respectively.

Figure 2 illustrates the fundamental structure of a single-branch SIR. An even-odd mode equivalent transmission line model is employed to analyze its resonance conditions [6]. Within this framework, the single branch is characterized by an admittance Y_2 and an electrical length θ_2. Correspondingly, the stepped-impedance section is defined by characteristic admittances Y_4 and Y_5, with respective electrical lengths θ_4 and θ_5.

The odd-mode admittance is:

$$Y_{\text{in,odd}} = jY_1 \frac{Y_2 \tan\theta_2 - Y_1 \cot\theta_3 + Y_1 \tan\theta_1}{Y_1 - (Y_2 \tan\theta_2 - Y_1 \cot\theta_3)\tan\theta_1} \tag{1}$$

The even-mode admittance is:

$$Y_{\text{in,even}} = Y_1 \frac{Y_{1\text{e}} + jY_1 \tan\theta_1}{Y_1 + jY_{1\text{e}} \tan\theta_1} \tag{2}$$

$$Y_{1\text{e}} = jY_2 \tan\theta_2 + Y_1 \frac{Y_{2\text{e}} + jY_1 \tan\theta_2}{Y_1 + jY_{2\text{e}} \tan\theta_2} \tag{3}$$

$$Y_{2\text{e}} = Y_4 \frac{Y_{3\text{e}} + jY_4 \tan\theta_4}{Y_4 + jY_{3\text{e}} \tan\theta_4} \tag{4}$$

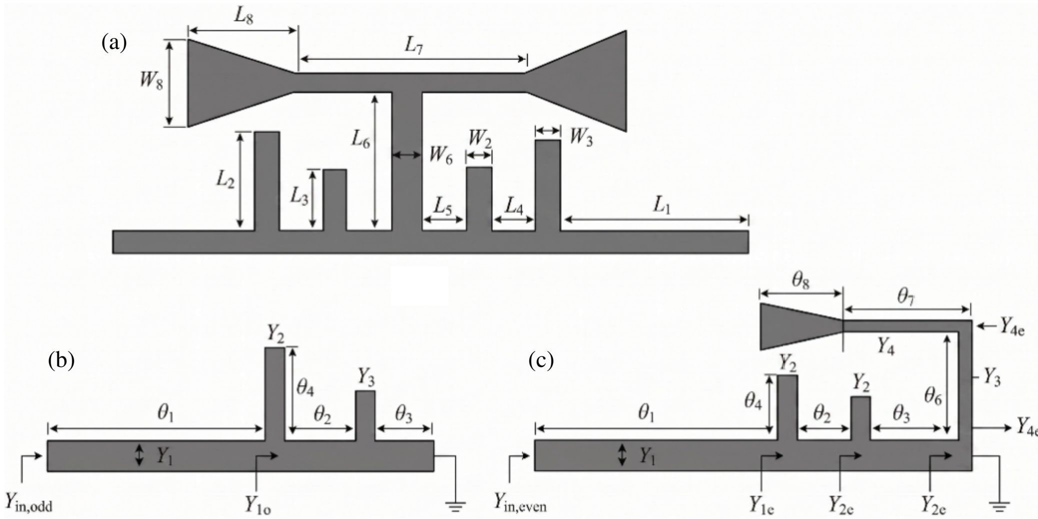

FIGURE 3. Equivalent circuit of the SIR parity mode with a single branch loaded. (a) Schematic diagram, (b) odd-mode equivalent circuit, and (c) even-mode equivalent circuit.

$$Y_{3\mathrm{e}} = jY_5 \tan\theta_5 \tag{5}$$

By applying the odd-mode resonance condition, $\mathrm{Im}[Y_{\mathrm{in,odd}}] = 0$, the following equation can be derived:

$$Y_1 - Y_2 \tan\theta_2 \tan\theta_3 - Y_1 \tan\theta_1 \tan\theta_3 = 0 \tag{6}$$

By applying the even-mode resonance condition, $\mathrm{Im}[Y_{\mathrm{in,even}}] = 0$, the following equation can be derived:

$$Y_{1e} + jY_1 \tan\theta_1 = 0 \tag{7}$$

As indicated by Equation (6), the odd-mode resonance frequency is governed exclusively by the uniform-impedance branch and remains independent of the stepped-impedance section. Consequently, this frequency can be systematically tuned by adjusting the structural parameters (θ_1, Y_1) of the uniform branch. Conversely, Equation (7) demonstrates that the even-mode resonance frequency is jointly determined by the physical dimensions of both the stepped-impedance section (Y_2, θ_2, Y_3, θ_3) and the uniform-impedance branch (Y_1, θ_1). Building upon the aforementioned multimode resonator, an enhanced configuration is developed by substituting the conventional stepped-impedance resonator (SIR) with a bowtie SIR. Furthermore, the design incorporates two pairs of uniform-impedance branches — replacing the original single pair — which are symmetrically loaded on both sides of the central bowtie structure. The fundamental geometric layout and the corresponding even- and odd-mode equivalent circuits are illustrated in Fig. 3. Specifically, the characteristic admittances of the two pairs of uniform-impedance lines are denoted as Y_{b1} and Y_{b2}, with corresponding electrical lengths of θ_{b1} and θ_{b2}, respectively. Furthermore, the distinct sections of the dumbbell-shaped stepped-impedance resonator (SIR) exhibit characteristic admittances of Y_{s1} and Y_{s2}, corresponding to electrical lengths of θ_{s1} and θ_{s2}, respectively [7, 8].

Under even-mode excitation, based on transmission line theory, the even-mode input admittance, $Y_{\mathrm{in,even}}$, can be derived as follows:

$$Y_{\mathrm{in,even}} = Y_1 \frac{Y_{1e} + jY_1 \tan\theta_1}{Y_1 + jY_{1e} \tan\theta_1} \tag{8}$$

Among them

$$Y_{1e} = jY_2 \tan\theta_4 + Y_1 \frac{jY_{2e} + jY_1 \tan\theta_2}{Y_1 + jY_{2e} \tan\theta_3} \tag{9}$$

$$Y_{2e} = jY_2 \tan\theta_5 + Y_1 \frac{jY_{3e} + jY_1 \tan\theta_3}{Y_1 + jY_{3e} \tan\theta_3} \tag{10}$$

$$Y_{3e} = Y_3 \frac{jY_{4e} + jY_3 \tan\theta_6}{Y_1 + jY_{4e} \tan\theta_6} \tag{11}$$

$$Y_{4e} = jY_4 \frac{Y_5 \tan\theta_8 + Y_4 \tan\theta_7}{Y_4 - Y_5 \tan\theta_8 \tan\theta_7} \tag{12}$$

Under odd-mode excitation, based on transmission line theory, the odd-mode input admittance, $Y_{\mathrm{in,odd}}$, can be derived as follows:

$$Y_{\mathrm{in,odd}} = Y_1 \frac{Y_{1o} + jY_1 \tan\theta_1}{Y_1 + jY_{1o} \tan\theta_1} \tag{13}$$

$$Y_{1o} = jY_2 \tan\theta_4 + Y_1 \frac{jY_2 \tan\theta_5 - jY_1 \cot\theta_3 + jY_1 \tan\theta_2}{Y - Y_2 \tan\theta_5 - jY_1 \cot\theta_3 \tan\theta_2} \tag{14}$$

By applying the even- and odd-mode resonance conditions, $\mathrm{Im}[Y_{\mathrm{in,even}}] = 0$ and $\mathrm{Im}[Y_{\mathrm{in,odd}}] = 0$, to Equations (8) and (14), the respective resonance equations can be derived as follows:

$$Y_{1e} + jY_1 \tan\theta_1 = 0 \tag{15}$$

$$Y_{1o} + jY_1 \tan\theta_1 = 0 \tag{16}$$

As indicated by Equations (16) and (17), both the odd- and even-mode resonance frequencies depend on the uniform-impedance branches (L_2, W_2). However, the dumbbell-shaped stepped-impedance section (L_7, L_8, W_7, W_8) exclusively influences the even-mode resonance frequency. Consequently, modifying the physical parameters of the central bowtie stepped-impedance resonator alters only the even-mode response, leaving the odd-mode resonance entirely unaffected.

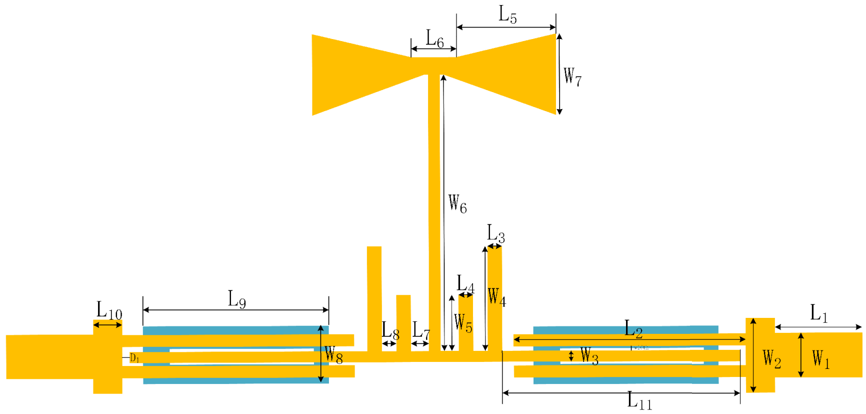

FIGURE 4. Equivalent circuit of the SIR parity mode with a single branch loaded.

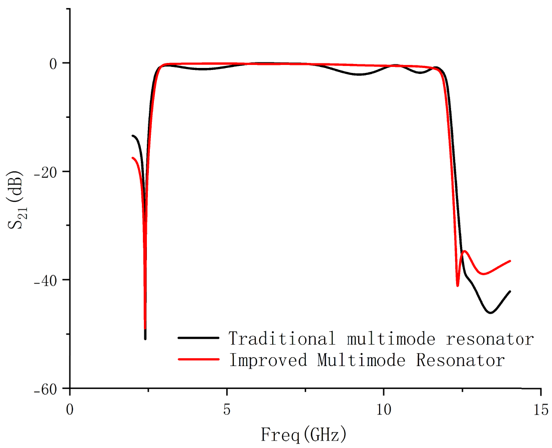

FIGURE 5. Comparison of S_{21} parameters for two ultra-wideband filters.

Although slightly more structurally complex than the preceding architecture, this proposed design offers significantly enhanced flexibility for frequency tuning.

Based on the preceding analysis, Fig. 4 illustrates the schematic configuration of the enhanced multimode resonator-based ultra-wideband (UWB) filter. This multimode resonator comprises a bowtie-shaped, stepped-impedance open-circuited branch positioned in the central plane, which is symmetrically loaded on either side with uniform-impedance branches of varying lengths. Additionally, the filter utilizes a parallel-coupled feeding structure, beneath which two annular defected ground structures are etched to substantially enhance the overall coupling strength. This configuration minimizes the requisite etched area, mitigates in-band insertion loss, and flattens the passband ripple, thereby yielding an ultra-wideband (UWB) filter with superior filtering characteristics.

The proposed filter was modeled and evaluated using the electromagnetic simulation software Ansys HFSS 19.0. The design was implemented on a Rogers 5880 substrate, characterized by a thickness of 0.762 mm, a relative permittivity of 2.2, and a loss tangent of 0.0009. Following iterative optimization, the final physical dimensions were established as follows (in mm): $L_1 = 3$, $L_2 = 8$, $L_3 = 0.5$, $L_4 = 0.5$, $L_5 = 3.42$, $L_6 = 1.56$, $L_7 = 0.62$, $L_8 = 0.5$, $L_9 = 6.4$, $L_{10} = 1$, $L_{11} = 8.2$, $W_1 = 1.5$, $W_2 = 2.5$, $W_3 = 0.4$, $W_4 = 3.6$, $W_5 = 1.93$, $W_6 = 9.5$, $W_7 = 2.8$, $W_8 = 2$, width $= 0.13$, and $D_1 = 0.21$.

Compared to designs previously reported in the literature, the proposed configuration introduces three principal structural enhancements: first, the substitution of the conventional rectangular stepped-impedance resonator (SIR) with a bowtie SIR; second, the transition from a single-branch to a multi-branch loading scheme; and third, the replacement of the rectangular defected ground structure (DGS) with an annular DGS. Fig. 5 compares the S-parameters of the two distinct designs. As evidenced by the transmission characteristics, the enhanced multimode resonator demonstrates superior passband flatness and reduced insertion loss across the UWB frequency range of 2.7 to 12.0 GHz. Crucially, this design effectively suppresses the response fluctuations previously observed near 9.5 GHz in the conventional architecture. Although the proposed structure exhibits a marginally shallower upper-stopband rejection depth above 12.5 GHz relative to the traditional design, it provides a significantly sharper edge roll-off. Overall, the enhanced configuration successfully optimizes in-band transmission, achieving a highly flat passband response while simultaneously maintaining robust out-of-band rejection.

3. DESIGN OF A QUAD-NOTCH ULTRA-WIDEBAND FILTER

Building upon the proposed ultra-wideband (UWB) filter utilizing a bowtie multimode resonator, this section details the introduction of multiple band-notched characteristics via the asymmetric coupling of external resonant structures. Specifically, a single notch is generated by integrating an open-circuited branch above the primary resonator, and three additional notches are realized by coupling a novel quasi-closed-loop C-shaped resonator beneath it. This strategic configuration ultimately yields a quad-notch UWB filter.

The formation of the initial notch is governed by an asymmetric coupling structure. Fig. 6 presents the schematic of a single-notch UWB filter, wherein an auxiliary branch is integrated into the fundamental UWB architecture to introduce a transmission zero within the passband. This structural modi-

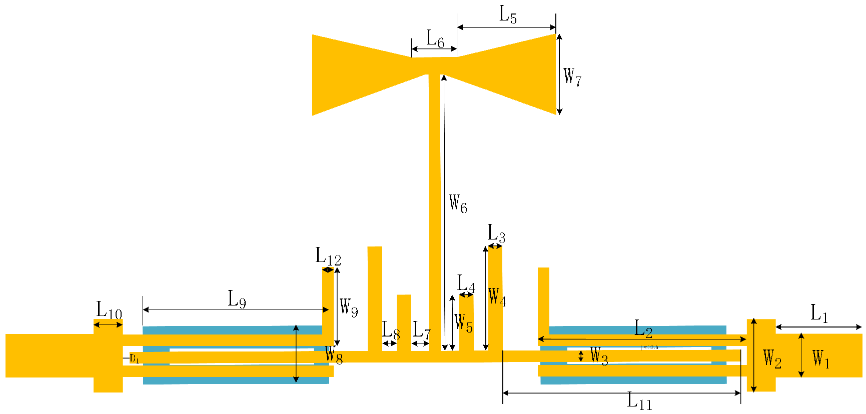

FIGURE 6. Schematic diagram of a single-notch ultra-wideband filter.

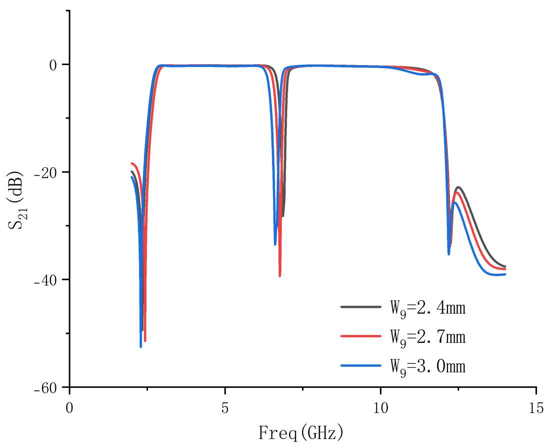

FIGURE 7. Effect of the length of W_9 on the notch filter.

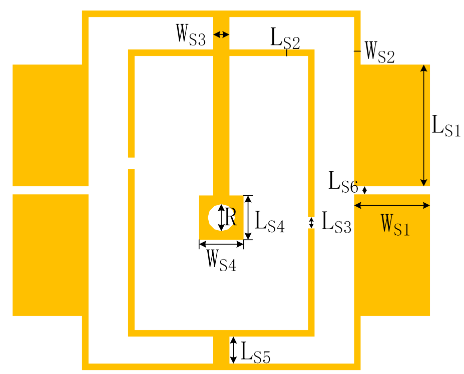

FIGURE 8. C-type resonator.

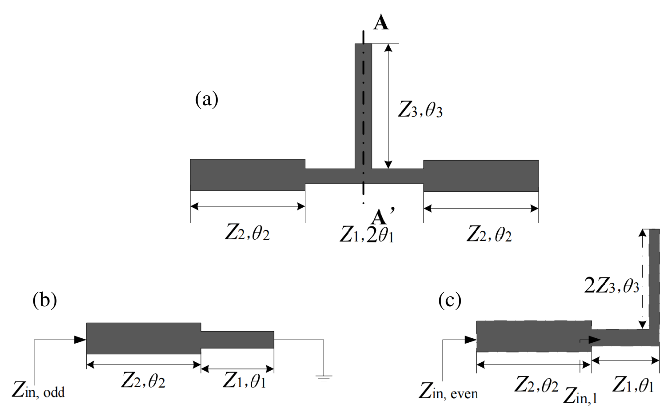

FIGURE 9. Structure diagram and odd-even mode equivalent analysis of the UISL-SIR. (a) Structure diagram, (b) odd-mode equivalent analysis, and (c) even-mode equivalent analysis.

fication yields a notch depth of 39.39 dB at 6.76 GHz, thereby effectively mitigating interference from the Fixed Satellite Service (FSS) uplink and safeguarding the overall UWB system [9].

The dimensions of the auxiliary branch, particularly its length and width, critically govern the notch performance. Fig. 7 illustrates the effect of varying the length parameter W_9 on the notch characteristics. The results demonstrate that adjusting W_9 facilitates the precise tuning of the in-band notch near 6.7 GHz. Specifically, optimal performance is achieved at $W_9 = 2.7$ mm (red curve), yielding a peak attenuation approaching -40 dB and demonstrating the most robust interference suppression. In contrast, alternative parameter configurations exhibit notable performance degradations: at $W_9 = 2.4$ mm (black curve), the notch center frequency shifts upward with inadequate stopband attenuation (approximately -28 dB); conversely, at $W_9 = 3.0$ mm (blue curve), the notch center undergoes an excessive downward frequency shift, accompanied by a diminished notch depth and compromised isolation (approximately -32 dB).

To achieve an efficient transition from a single-notch to a quad-notch filtering response, this design abandons the conventional redundant strategy of stacking multiple resonant stubs and, instead, introduces a novel quasi-closed-loop C-shaped resonator unit, as illustrated in Fig. 8. From a topological perspective, the proposed resonator is not merely a simple geometrical combination; rather, it represents an ingeniously integrated composite structure consisting of a stepped-impedance resonator (SIR) loaded with a stepped-impedance stub, a uniformly impedance stub-loaded SIR (UISL-SIR), and an outer C-shaped coupling ring. Benefiting from this highly integrated physical architecture, three independently controllable resonant modes can be simultaneously excited within an extremely compact footprint, thereby enabling multiple notch bands with minimal circuit complexity and size penalty.

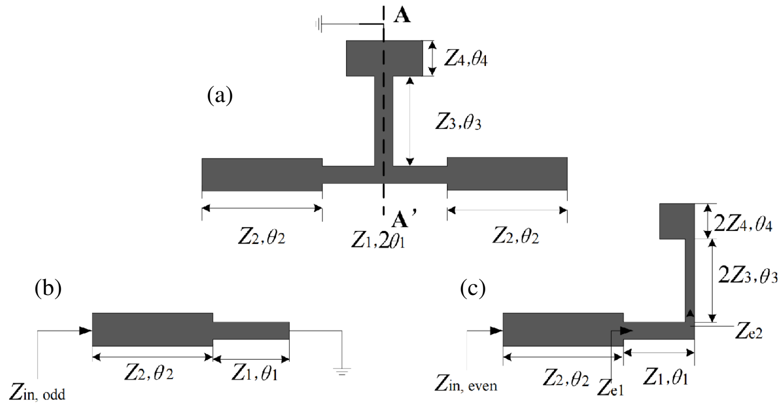

FIGURE 10. Basic structure and odd-even mode equivalent models of the SISL-SIR. (a) Structure of the SISL-SIR, (b) odd-mode equivalent analysis, and (c) even-mode equivalent analysis.

In the design of the multi-notch ultra-wideband bandpass filter, the outer configuration of the approximately closed-loop C-shaped resonator (ACLC-SIR) is symmetrically constructed by combining an open-ended uniform-impedance-stub-loaded stepped-impedance resonator (UISL-SIR) and a short-ended stepped-impedance-stub-loaded stepped-impedance resonator (SISL-SIR). Owing to the strict geometrical symmetry of the proposed structure with respect to the central reference plane, the odd-even mode analysis method is employed to decompose the resonator into two independent equivalent transmission-line models corresponding to the odd and even modes. This approach enables effective extraction and decoupling of key parameters governing individual resonant frequencies, providing valuable theoretical guidance for the precise control and optimization of multiple notch characteristics. The structures of the UISL-SIR and SISL-SIR are shown in Fig. 9 and Fig. 10, respectively.

Under odd-mode excitation, no current flows through the central symmetry plane of the proposed structure, which can be equivalently regarded as an ideal electric wall (short circuit). For both the UISL-SIR and SISL-SIR configurations, the characteristic impedances of the main stepped-impedance resonator (SIR) are denoted as Z_1 and Z_2, while the corresponding electrical lengths are represented by θ_1 and θ_2, respectively.

$$Z_{\text{in,odd}} = jZ_1 \frac{Z_1 \tan\theta_1 + Z_2 \tan\theta_2}{Z_1 - Z_2 \tan\theta_1 \tan\theta_2}. \tag{17}$$

According to the fundamental theory of resonant networks, the odd-mode resonance condition can be obtained by setting the imaginary part of the input admittance to zero, i.e.,

$$\text{Im}\left[\frac{1}{Z_{\text{in,odd}}}\right] = 0. \tag{18}$$

Consequently, the odd-mode resonant condition is derived as

$$\tan\theta_1 \tan\theta_2 = \frac{Z_1}{Z_2}. \tag{19}$$

It can be observed from the above resonance equation that, regardless of the open-ended UISL-SIR or short-ended SISL-SIR, the odd-mode resonant frequencies are solely determined by the characteristic impedance ratio and electrical lengths of the main SIR. In particular, they are completely independent of the physical dimensions of the loaded stub, including the uniform open-ended stub and the stepped-impedance shorted stub.

Under even-mode excitation, the electric fields are symmetric with respect to the central plane, which can be equivalently modeled as an ideal magnetic wall (open circuit). In this case, the parameters of the loaded stubs directly participate in the derivation of the resonance conditions. For the open-ended UISL-SIR configuration, the characteristic impedance and electrical length of the loaded uniform impedance open stub are defined as Z_3 and θ_3, respectively. The impedance ratios are introduced as

$$R_{Z1} = \frac{Z_2}{Z_1}, \tag{20}$$

$$R_{Z2} = \frac{Z_1}{Z_3}. \tag{21}$$

By imposing the even-mode resonance condition

$$\text{Im}\left[\frac{1}{Z_{\text{in,even}}}\right] = 0, \tag{22}$$

the corresponding resonance equation of the UISL-SIR can be obtained as

$$\begin{aligned} &2R_{Z1}\tan\theta_1 + 2\tan\theta_2 + R_{Z1}R_{Z2}\tan\theta_3 \\ =\ &R_{Z2}\tan\theta_1\tan\theta_2\tan\theta_3. \end{aligned} \tag{23}$$

For the short-ended SISL-SIR configuration, the characteristic impedances of the loaded stepped-impedance stub are defined as Z_3 and Z_4, with corresponding electrical lengths θ_3 and θ_4. The impedance ratio is defined as

$$R_{Z3} = \frac{Z_3}{Z_4}. \tag{24}$$

By solving the even-mode resonance equation and performing mathematical simplification, the resonance condition of the SISL-SIR can be expressed as

$$R_{Z2}(R_{Z1} - \tan\theta_1\tan\theta_2)(R_{Z3} - \tan\theta_3\tan\theta_4)$$

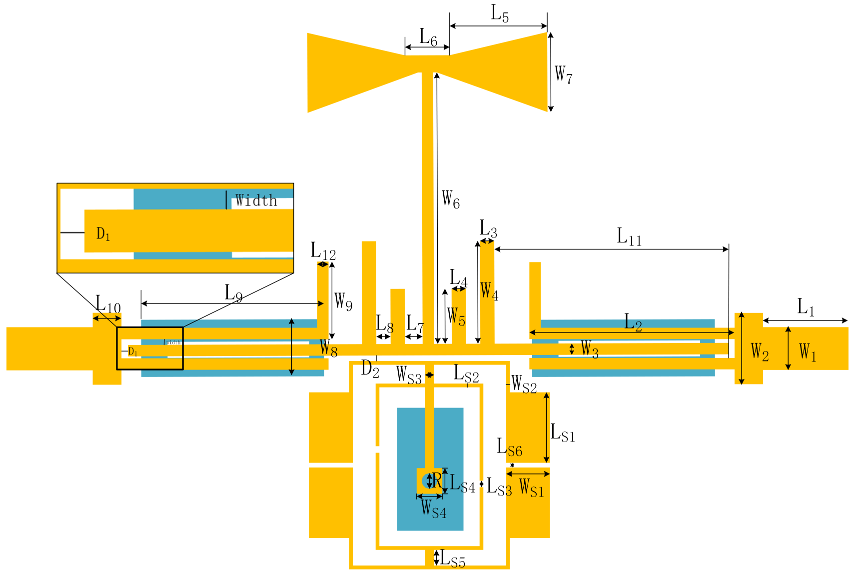

FIGURE 11. Schematic diagram of a quad-notch ultra-wideband filter design.

$$= 2(R_{Z1}\tan\theta_1 + \tan\theta_2)(R_{Z3}\tan\theta_3 + \tan\theta_4). \quad (25)$$

Unlike the odd-mode characteristics, even-mode resonant frequencies of the UISL-SIR and SISL-SIR structures are not only determined by the dimensions of the main SIR but also strongly dependent on the impedance ratios and electrical lengths of the loaded stubs.

Based on the above analysis, the proposed ACLC-SIR structure exhibits remarkable resonant frequency decoupling characteristics. Specifically, variations in the physical parameters of the loaded stubs only affect the even-mode resonant frequencies, while the odd-mode resonances remain completely immune to these variations. This decoupling mechanism provides important theoretical guidance for the synthesis of multimode resonators (MMRs) and subsequent full-wave electromagnetic optimization. During the optimization of the transmission characteristics of the microstrip filter, such as the S_{11} and S_{21} responses, a stepwise tuning strategy can be adopted:

Odd-mode tuning: The odd-mode resonance frequencies can be accurately positioned by adjusting the impedance ratio (K value) and physical length of the main SIR structure.

Even-mode tuning: The even-mode resonances can subsequently be independently optimized by modifying the geometrical parameters of the externally loaded stubs, such as their lengths and widths, thereby providing flexible control over the resonant frequencies and notch depths.

Through this design methodology, compact, high-performance multi-notch wideband filtering responses can be achieved without increasing the circuit's overall footprint.

A quad-notch filter is realized by coupling the complete C-shaped resonant unit beneath the single-notch filter and incorporating a rectangular defected ground structure (DGS). The proposed structural model is illustrated in Fig. 11. However, direct coupling may induce mutual interference among the respective notches, consequently degrading the overall frequency response. To mitigate this issue, a rectangular ground plane is introduced underneath, and both the coupling spacing and device parameters are iteratively optimized to achieve optimal simulation results. Fig. 12(a) presents the simulated S-parameters of the complete filter obtained via HFSS. The results indicate that the proposed quad-notch ultra-wideband (UWB) filter exhibits excellent transmission and matching characteristics across the target passband of 2.7–11.8 GHz. In the non-notch regions, the insertion loss (S_{21}) is maintained above -1.0 dB, while the return loss (S_{11}) remains consistently below -10 dB. To mitigate multi-source radio frequency (RF) interference, the design successfully generates four independent, steep-edged narrowband notches at 6.14 GHz, 7.02 GHz, 7.56 GHz, and 8.41 GHz. The attenuation level at each notch frequency drops below -17 dB, with a peak attenuation reaching -38 dB, thereby providing effective isolation against typical narrowband interfering signals, including WLAN and X-band transmissions. Moreover, the proposed filter maintains exceptional amplitude-frequency flatness — with fluctuations below ± 0.5 dB outside the notch regions — and low group-delay distortion within the effective passband. Concurrently, it introduces deep transmission zeros at both the lower (2.3 GHz) and upper (12.3 GHz) out-of-band margins, substantially enhancing out-of-band suppression and the stopband roll-off rate. Following the integration of the C-shaped resonator, the operational passband narrowed marginally from 2.7–12.0 GHz to 2.7–11.8 GHz. This bandwidth reduction is attributed to the adjustment of the overall coupling spacing, which was necessitated to achieve optimal attenuation across the three corresponding notches. Despite this minor bandwidth degradation, the trade-off remains highly justifiable within the design paradigm, as it enables the successful realization of a quad-notch frequency response. In summary, this design successfully integrates multiple highly independent notches with minimal mutual interference, while preserving a compact physical footprint. The simulated performance demonstrates strong agreement with theoretical expectations, robustly validating the efficacy and advanced nature of the proposed multimode res-

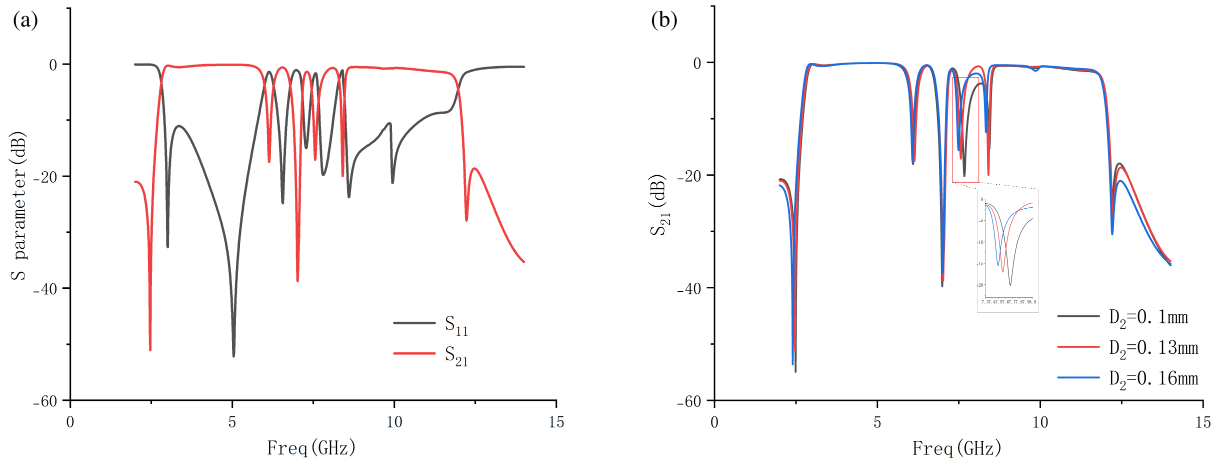

FIGURE 12. Simulation S-parameter results for a quad-notch ultra-wideband filter. (a) S-parameter comparison chart and (b) the effect of D_2 on S_{21} parameters.

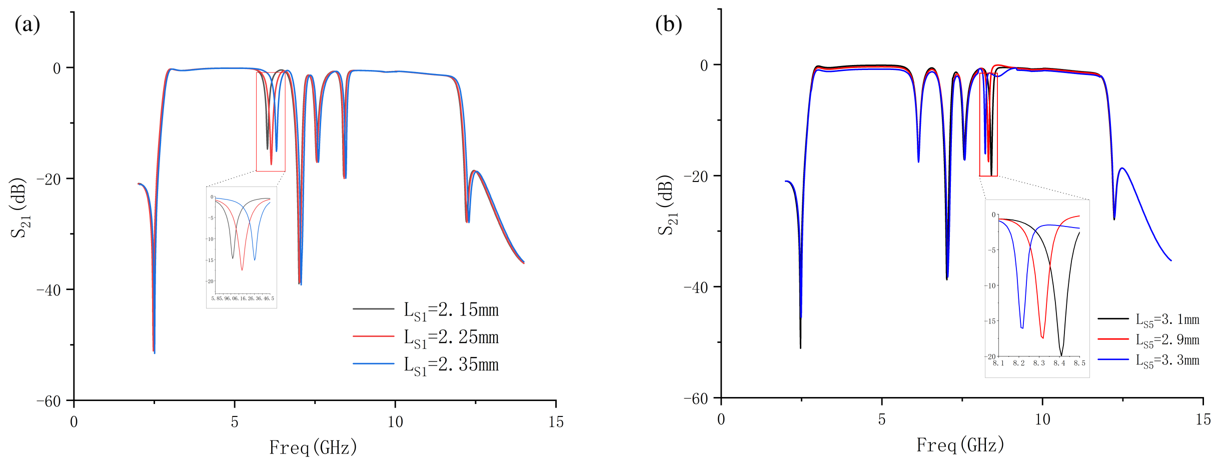

FIGURE 13. Effects of various parameters on simulation results. (a) The effect of L_{S1} on S_{21} parameters and (b) the effect of L_{S5} on S_{21} parameters.

onator and defected ground structure (DGS) for ultra-wideband anti-interference communication systems operating in complex electromagnetic environments.

The coupling distance between the C-shaped resonator and the improved multimode resonator plays a critical role in determining coupling strength and filtering characteristics. Therefore, a parametric study of D_2 was conducted, and the corresponding simulated results are presented in Fig. 12(b). It can be observed that the variation of D_2 has a negligible impact on the notch responses at 6.14 GHz and 7.02 GHz, and the higher-order notch modes located at 7.56 GHz and 8.41 GHz are significantly affected. This phenomenon indicates that the coupling distance primarily regulates the resonant modes associated with the C-shaped coupling structure while maintaining the stability of other resonances.

When $D_2 = 0.1$ mm, the notch depth at 7.56 GHz is enhanced; however, the transmission characteristic between 7.56 GHz and 8.41 GHz deteriorates significantly, resulting in an undesirable attenuation of approximately -3 dB. In contrast, when $D_2 = 0.16$ mm, the passband attenuation is improved, but additional perturbation appears around 9.88 GHz, leading to degraded passband flatness. After comprehensive consideration, $D_2 = 0.13$ mm achieves an optimal balance among coupling intensity, notch rejection, and passband stability.

To investigate the influence of the loaded stub length L_{S1} on the resonant characteristics, a parametric analysis was performed by varying L_{S1} from 2.15 mm to 2.35 mm. As shown in Fig. 13(a), changing L_{S1} primarily affects the notch resonance associated with this loaded stub, while the other notch frequencies remain almost unchanged. With increasing L_{S1}, the corresponding notch frequency shifts toward lower frequencies due to the increased equivalent electrical length and enhanced reactive loading.

The weak interaction between L_{S1} and remaining resonant modes demonstrates that the introduced resonance can be independently controlled. Meanwhile, the notch depth variation is mainly attributed to modification of the coupling strength between the resonator and the main transmission path. Therefore, L_{S1} provides an effective tuning degree of freedom for accurately positioning the specific notch band without deteriorating the overall filtering response.

Similarly, the effect of L_{S5} on the high-frequency notch response was investigated by varying its value from 2.9 mm to

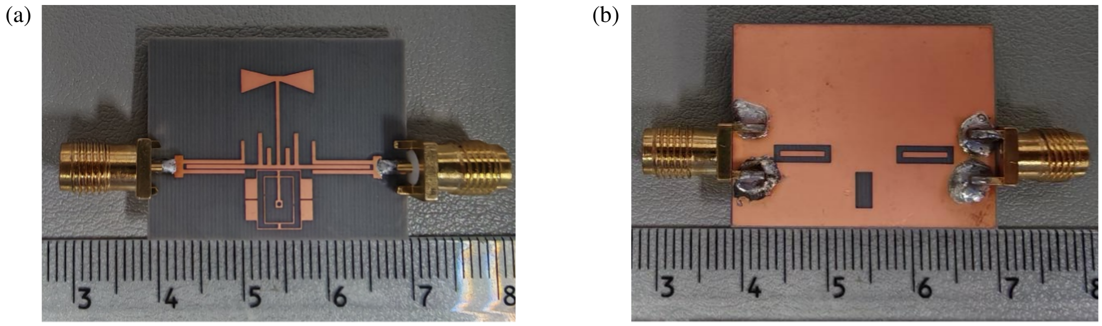

FIGURE 14. Photographs of the fabricated device. (a) Front view showing the microstrip line structure and (b) back view showing the rectangular defect region.

3.3 mm. As depicted in Fig. 13(b), L_{S5} predominantly controls the fourth notch located around 8.3 GHz, and the other resonant modes and the UWB passband characteristics remain almost unchanged. As L_{S5} increases, the notch frequency moves toward lower frequencies, which can be attributed to the increased electrical length of the resonant path.

Furthermore, the L_{S5} variation slightly influences the notch depth due to the change in coupling strength. An optimized value of $L_{S5} = 3.1$ mm provides the desired notch location and sufficient rejection level, demonstrating the effectiveness of this parameter in independently regulating the high-frequency notch characteristic.

The above parametric analyses reveal that the proposed ACLC-SIR resonator possesses remarkable multi-mode frequency-decoupling capability. Specifically, the parameters D_2, L_{S1}, and L_{S5} provide independent control over different resonant modes, enabling flexible adjustment of multiple notch bands without significant interaction among them. This characteristic originates from the unique composite topology of the quasi-closed-loop C-shaped resonator, in which different resonant paths are spatially integrated while maintaining electrical independence. Compared with conventional multi-notch filters relying on multiple cascaded or stacked resonators, the proposed structure achieves compact size, reduced design complexity, and enhanced modal controllability. Therefore, the ACLC-SIR provides an effective approach for realizing high-performance UWB bandpass filters with independently tunable multi-notch characteristics.

Based on the preceding theoretical analysis, the proposed filter was modeled and optimized using the electromagnetic simulation software HFSS 19.0. The final physical dimensions (in millimeters) are as follows: $L_1 = 3$, $L_2 = 8$, $L_3 = 0.5$, $L_4 = 0.5$, $L_5 = 3.42$, $L_6 = 1.56$, $L_7 = 0.62$, $L_8 = 0.5$, $L_9 = 6.4$, $L_{10} = 1$, $L_{11} = 8.2$, $W_1 = 1.5$, $W_2 = 2.5$, $W_3 = 0.4$, $W_4 = 3.6$, $W_5 = 1.93$, $W_6 = 9.5$, $W_7 = 2.8$, $W_8 = 2$, width $= 0.13$, $D_1 = 0.21$, $L_{12} = 5.2$, $L_{13} = 3.4$, $L_{14} = 3.4$, $L_{15} = 2.4$, $W_9 = 2.7$, $W_{10} = 1.2$, $W_{11} = 1.2$, $W_{12} = 1.4$, $W_{13} = 2.4$, $W_{14} = 2.0$, $D_2 = 0.13$, and $D_3 = 0.21$. The device was fabricated on a Rogers 5880 substrate with a thickness of 0.762 mm, a relative permittivity of 2.2, and a loss tangent of 0.0009. The fabricated prototype is presented in Fig. 14, wherein Fig. 14(a) displays the top microstrip layer, and Fig. 14(b) illustrates the bottom ground plane.

To experimentally evaluate the practical performance of the proposed quad-notch UWB filter, the fabricated prototype was characterized using a professional microwave measurement setup. The experimental S-parameters were measured using a Ceyear 3674H vector network analyzer (VNA). Before the device testing, a full two-port Short-Open-Load-Thru (SOLT) calibration procedure was systematically implemented to ensure measurement accuracy across the entire frequency band of interest. Furthermore, to eliminate parasitic effects, phase shifts, and insertion losses introduced by the testing fixtures and SMA connectors, a de-embedding process was carefully performed, thereby shifting the measurement reference planes precisely to the actual input and output ports of the filter prototype.

As illustrated in Fig. 15, the measured results obtained using this setup (solid lines) exhibit strong agreement with simulated ones (dashed lines). The simulated center frequencies for the four notches are 6.15 GHz, 7.01 GHz, 7.57 GHz, and 8.41 GHz, and the corresponding measured values are 5.91 GHz, 6.75 GHz, 7.29 GHz, and 8.08 GHz. The measured 3-dB fractional bandwidths for these notches are 3.64% (5.75–6.07 GHz), 4.56% (6.53–6.93 GHz), 3.87% (7.14–7.48 GHz), and 2.05% (7.99–8.17 GHz), respectively, with corresponding rejection depths reaching 15.63 dB, 34.55 dB, 15.01 dB, and 15.82 dB. Furthermore, the measured passband extends from 2.71 GHz to 11.5 GHz (compared to the simulated range of 2.92–11.88 GHz). Operating at a center frequency of 7.11 GHz, the filter achieves a 3-dB fractional bandwidth of 124%, substantially exceeding the standard ultra-wideband (UWB) spectrum of 3.1–10.6 GHz. The overall physical dimensions of the device are 23 mm × 29.74 mm ($0.67\lambda_g \times 0.81\lambda_g$). Notably, the proposed quad-notch filter architecture offers exceptional design flexibility, as it can be independently configured to realize single- or triple-notch responses based on specific application requirements. Minor discrepancies observed between the measured and simulated S-parameters can be primarily attributed to manufacturing tolerances and mutual interference among the notches; nevertheless, the overall experimental results demonstrate strong agreement with the simulations. In addition, the group-delay characteristics of the proposed filter were also investigated. As shown in Fig. 15, the measured group delay remains relatively flat within the UWB passband, indicating sta-

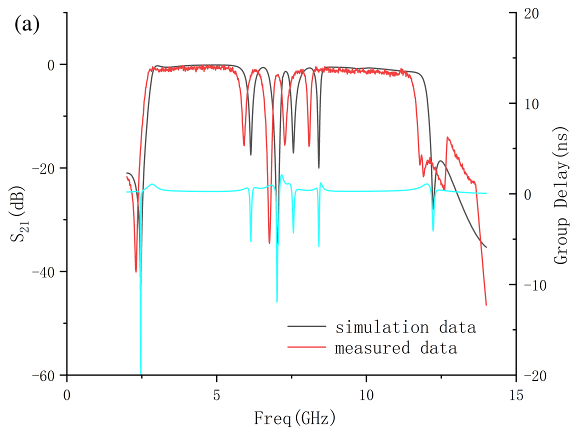

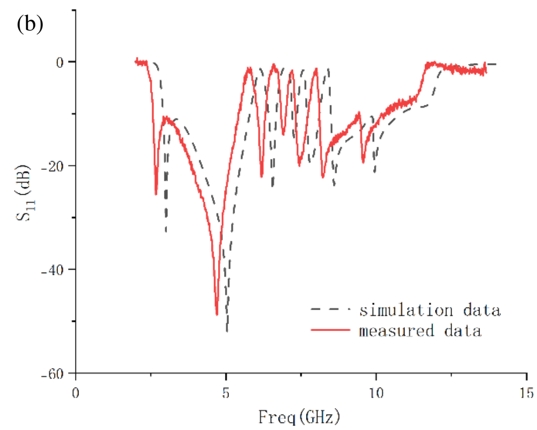

FIGURE 15. Comparison of test simulation results: (a) Comparison with S_{21} and (b) Comparison with S_{11}.

TABLE 1. Comparison of the multi-notch ultra-wideband filter proposed in this paper with those in other literature.

References	Relative permittivity (ε_r)	Passband (GHz)	Notch frequency (GHz)/ Attenuation (dB)	Blockband suppression (dB)	Machining dimensions (λ_g)	Maximum number of notches introduced by a single resonator
[10]	3.38	3.1–10.4	5.3, 6.4, 7.4/> 15	17	0.61×0.34	1
[11]	3.66	2.8–10.6	3.3, 5.1, 8.3/> 15	Unknown	0.06×0.02	1
[12]	4.4	2.8–10.2	4.4, 5.3, 8.2/> 10	20	0.37×0.18	1
[13]	3.55	2.81–10.2	5.29, 5.83, 7.99	15	0.94×1	1
[14]	10.8	3.25–10.73	5.6, 6.42, 8.03/> 19	17	1.04×0.66	1
[15]	2.2	3.2–12.4	5.18, 5.86, 7.92/> 16	15.3	0.71×0.34	1
This paper	2.2	2.71–11.5	5.91, 6.75, 7.29, 8.08/> 15	34.55	0.67×0.81	3

ble signal transmission performance and low phase distortion. Although sharp variations in group delay are observed around the notch frequencies due to the strong coupling effect of the introduced resonant units, the delay fluctuation is mainly confined to the rejected bands and has negligible influence on the in-band signal integrity. These results further verify the excellent filtering performance and practical applicability of the proposed quad-notch UWB filter for high-speed wireless communication systems.

Table 1 presents a performance comparison between the proposed quad-notch filter and other UWB filters reported in the literature. The key parameters evaluated include passband bandwidth, notch center frequencies, stopband rejection levels, physical dimensions, and the maximum number of notches introduced by a single resonator. The comparative data demonstrate that, despite a relatively larger footprint, the proposed design achieves a greater number of notches, enhanced rejection depths, and a broader passband. Consequently, the proposed filter successfully integrates multiple rejection bands while simultaneously delivering superior stopband attenuation and an extended operational bandwidth. Minor discrepancies observed between the measured and simulated S-parameters can be primarily attributed to manufacturing tolerances and mutual interference among the notches; nevertheless, the overall experimental results demonstrate strong agreement with the simulations.

4. CONCLUSION

To achieve multi-band notch suppression within an ultra-wideband (UWB) filter while maintaining a wide passband and high frequency selectivity, this study proposes a quad-notch UWB filter based on a bowtie T-shaped resonator. Experimental results demonstrate an operational passband of 2.71–11.5 GHz, corresponding to a 3-dB fractional bandwidth of 124% and a bandpass selectivity of 0.944. To effectively mitigate fixed interference signals, such as WLAN and X-band satellite communications, an open-loop branch and a novel closed-loop C-shaped resonant unit are integrated into the fundamental UWB architecture. This configuration successfully generates four independent notches with measured center frequencies at 5.91 GHz, 6.75 GHz, 7.29 GHz, and 8.08 GHz. The corresponding rejection depths exceed 15 dB (reaching a peak attenuation of 34.55 dB), thereby ensuring robust suppression of multiple narrowband interferers. The fabricated prototype features a compact footprint of 23 mm $\times$ 29.74 mm (approximately $0.67\lambda_g \times 0.81\lambda_g$). By strategically employing miniaturization and performance-enhancement techniques — including the bowtie T-shaped resonator, branch-loaded notches, and a defected ground structure (DGS) — this work provides a highly effective solution for developing high-performance, multi-notch UWB filters. Furthermore, future research will focus on extending this design methodology to realize penta-notch and hexa-notch configurations by introducing additional decoupled loading stubs or nested multi-mode rings, thereby providing enhanced multi-band interference immunity for more complex electromagnetic environments.

ACKNOWLEDGEMENT

This work was financially supported by the University-Local Government Scientific and Technical Cooperation CultivationPproject of Ordos Institute-LNTU (Grant No. YJY-XD-2024-B-009).

REFERENCES

[1] Zhu, L., S. Sun, and W. Menzel, "Ultra-wideband (UWB) bandpass filters using multiple-mode resonator," *IEEE Microwave and Wireless Components Letters*, Vol. 15, No. 11, 796–798, 2005.

[2] Fakharian, M. M., P. Rezaei, A. A. Orouji, and M. Soltanpur, "A wideband and reconfigurable filtering slot antenna," *IEEE Antennas and Wireless Propagation Letters*, Vol. 15, 1610–1613, 2016.

[3] Fakharian, M. M., "Compact multimode bandpass plasmonic filter based on a dual-spiral resonator coupled to metal-insulator-metal waveguides for refractive index sensing application," *Applied Optics*, Vol. 65, No. 16, 5695–5702, 2026.

[4] Chu, Q.-X., X.-H. Wu, and X.-K. Tian, "Novel UWB bandpass filter using stub-loaded multiple-mode resonator," *IEEE Microwave and Wireless Components Letters*, Vol. 21, No. 8, 403–405, 2011.

[5] Ahn, D., J.-S. Park, C.-S. Kim, J. Kim, Y. Qian, and T. Itoh, "A design of the low-pass filter using the novel microstrip defected ground structure," *IEEE Transactions on Microwave Theory and Techniques*, Vol. 49, No. 1, 86–93, 2001.

[6] Gao, M., Y. He, J. Nan, Z. Yang, and C. Wang, "A miniaturized ultra-wideband filter with high rejection and selectivity based on dual-notch bands," *PLoS ONE*, Vol. 19, No. 8, e0306730, 2024.

[7] Rai, J. K., D. K. Choudhary, P. Ranjan, and R. Chowdhury, "A compact ultrawide bandpass filter along Notch characteristics with rectangular resonator through a machine learning approach," *International Journal of Microwave and Wireless Technologies*, Vol. 16, No. 8, 1414–1422, 2024.

[8] Makimoto, M. and S. Yamashita, *Microwave Resonators and Filters for Wireless Communication: Theory, Design and Application*, Springer Science & Business Media, 2013.

[9] Shaman, H. and J.-S. Hong, "Ultra-wideband (UWB) bandpass filter with embedded band notch structures," *IEEE Microwave and Wireless Components Letters*, Vol. 17, No. 3, 193–195, 2007.

[10] Liu, F. and M. Qun, "A new compact UWB bandpass filter with quad notched characteristics," *Progress In Electromagnetics Research Letters*, Vol. 88, 83–88, 2020.

[11] Taibi, A., M. Trabelsi, and A. A. Saadi, "Efficient design approach of triple notched UWB filter," *AEU — International Journal of Electronics and Communications*, Vol. 131, 153619, 2021.

[12] Wang, L., S. Yang, Q. Guo, B. Li, and L. Zhang, "Super compact and ultra-wideband bandpass filter with three band notches using triple-mode stepped impedance resonator and defected ground structure," *Journal of Electromagnetic Waves and Applications*, Vol. 38, No. 10, 1158–1175, 2024.

[13] Mohamed, A., K. Djamel, F. Khelil, and F. Fouad, "A bandpass filter with triple-narrow notch bands based on metamaterials SRR configurations for UWB applications," *International Journal of Microwave & Optical Technology*, Vol. 19, No. 3, 244, 2024.

[14] Borhani, S. J., M. A. Honarvar, and B. S. Virdee, "Quad notched-band UWB BPF based on quintuple-mode resonator," *International Journal of Microwave and Wireless Technologies*, Vol. 9, No. 7, 1433–1439, 2017.

[15] Sung, Y. J., "UWB bandpass filter with quad notched bands," *Microwave and Optical Technology Letters*, Vol. 56, No. 10, 2286–2289, 2014.